第 43 卷 第 2 期/2023 年 1 月/光学学报 研究论文

光学学报

基于氧化石墨烯/聚苯乙烯电光调制器的运转模式可切换光纤激光器

张晓颖[1]，常建华[1,2*]，戴腾飞[1,2]，苏友朋[1]，刘向[1]，倪海彬[1]

[1]南京信息工程大学电子与信息工程学院，江苏 南京 210044；

[2]南京信息工程大学江苏省大气环境与装备技术协同创新中心，江苏 南京 210044

摘要 利用电信号改变氧化石墨烯(GO)固有的光学吸收特性，可以实现对光纤锁模激光器输出性能的有效调控。在GO中引入聚苯乙烯(PS)纳米微球可以实现光波导结构，进而形成局域场并有效降低器件损耗。因此，采用微电子打印工艺制备了基于GO/PS的电光调制器，并以较低的泵浦功率(34.3 mW)实现了环形光纤激光器运转模式的主动调控。在0～20 V的调制电压下，激光器实现了连续波、调Q锁模、锁模三种运转模式的切换。所设计的全光纤电调制器件将锁模信号的脉冲宽度压缩到了20 ps，对应的重复频率为21.4 MHz。通过调控驱动电压，该器件的插入损耗从2.30 dB降低到了0.86 dB，平均输出功率从1.09 mW提升了1.52 mW。

关键词 激光器；光纤锁模激光器；电光调制器；模式切换；氧化石墨烯；聚苯乙烯

中图分类号 TN242 **文献标志码** A **DOI**：10.3788/AOS221323

1 引 言

被动锁模光纤激光器因结构紧凑、环境稳定性高和成本低等优势，在生物成像、激光医疗、光纤通信和材料加工等领域中得到了广泛应用[1]。目前，国内外研究者着重研究如何提高光纤激光器的性能，如提高输出功率和光束质量等。开发窄脉冲宽度、高峰值的超短脉冲(皮秒和飞秒量级)并进行小型化、实用化的研究也是重中之重[2]。大多数光纤激光器利用非线性光学材料作为可饱和吸收体(SA)实现被动锁模(ML)技术，从而获得超短脉冲[3]。近年来，随着二维材料的发展，石墨烯及其衍生物、半导体可饱和吸收镜(SESAM)、黑磷等已经被广泛应用于光学激光器中[4-7]。氧化石墨烯(GO)因其亲水性、易加工、非线性光学吸收特性和宽吸收光谱范围等优点开始被广泛应用在光学领域中[8]。基于GO的光纤激光器已经实现了不同的运转模式，如连续波(CW)、调Q锁模(QML)和连续锁模(CWML)等。然而，由于GO的可饱和吸收能力相对固定，故在不依靠外部调制器的情况下，很难实现激光系统的模式切换。

近几年，研究者们将小型化的电容结构器件与二维材料相结合，利用电信号实现了二维材料光学性能的调控[9-10]。这种全光纤电调制器件还可以作为可饱和吸收器，与光纤激光器系统高度集成。这类器件在光学领域的应用与发展，使通过电信号调制光纤激光器的运转模式成为可能。2015年，Gao等[11]揭示了外电场可以调制单层氧化石墨烯(mGO)透射光谱的机理。实验结果表明，在周期性外电场作用下，mGO的透射光谱表现出可逆调控的特性，并且其调制深度可达25%。2018年，Nair等[12]利用二硫化钼(MoS_2)量子点(QD)与聚合物P3HT[poly-(3-hexylthiophene)]在光纤中协同自组装，使其与原始P3HT纤维相比电导率提高了约82%。实验将这一现象归因于光激发电荷从P3HT到QD的有效转移，从而实现了光电特性的有效调控。2020年，Kovalchuk等[13]利用石墨烯电容器调控光纤激光器中超短脉冲的产生，并通过改变调制电压的方式实现了从CW到CWML的模式切换。虽然基于石墨烯材料的电调制器件已经得到了广泛的研究应用[14-15]，但是大规模生产石墨烯材料是非常困难的且价格昂贵。GO表面附着的含氧官能团会导致其电子结构变化并限制了其电学性能，进而容易引起较高的调制电压。因此，本文提出了使用GO材料和聚苯乙烯(PS)纳米微球结合的方法。根据光波导理论[16]，每个覆着GO的PS微球可以形成光波导结构，可以限制发散的倏逝光形成局域场，增强光与材料的作用面积。当施加驱动电压时，电场诱导的电荷转移

收稿日期：2022-06-15；**修回日期**：2022-07-10；**录用日期**：2022-07-18；**网络首发日期**：2022-07-28

基金项目：国家自然科学基金(61875089，62175114)

通信作者：*jianhuachang@nuist.edu.cn

改变了电荷分布。GO内部载流子浓度发生了变化，进而影响了GO的光学性质，但依然保持了足够水平的饱和吸收来启动脉冲的产生[17]。

基于此，本文利用微电子打印工艺展示了一种基于GO/PS的全光纤电容型可饱和吸收器件。这种电光调制器在较低的电调制功率下表现出可调的吸收特性，这归因于GO中的载流子浓度受电场影响发生了变化。将该器件引入到中心波长为1550 nm的环形光纤激光器中，成功实现了通过调控驱动电压的方式来确定全光纤锁模激光器的最佳工作模式。在34.3 mW的低泵浦功率下，激光器在0～20 V的驱动电压范围内实现了CW、QML、CWML的切换。这种全光纤电调制器件将CWML信号的脉冲宽度压缩到了20 ps，此时对应的重复频率为21.4 MHz。同时，该器件的插入损耗在驱动电压的调控下从2.30 dB降低到了0.86 dB，平均输出功率从1.09 mW提升到了1.52 mW。这种电光调制器的小体积、兼容性、宽光谱范围等优势有利于可调控光电子器件的应用与发展。

2　器件的制备与表征分析

电光调制器主要由GO/PS复合材料、聚甲基丙烯酸甲酯（PMMA）和氧化铟锡（ITO）构成。该器件为GO/PS-PMMA-ITO（GPI）的三明治结构，如图1(a)所示。GO/PS层的扫描电子显微镜（SEM）图像如图1(b)所示。可以看到，直径约为690 nm的单层PS微球均匀分散、分布排列，且薄片状的GO良好地覆盖在PS微球的表面上，这得益于GO表面负载的大量含氧官能团使其表现出了与聚合物的兼容性、吸附性和亲水性[18]。GPI器件主要由微电子打印机（上海幂方电子科技有限公司，MP1100）的喷墨打印、点胶等工艺制备完成。该工艺具有成本低、精度高和沉积速度快等优点。如图1(c)所示，主要制备步骤：1）采用微电子打印工艺依次在石英衬底上沉积185 nm厚的ITO、尺寸为5 mm×2 mm的银电极和200 nm厚的PMMA；2）将用强酸腐蚀过包层的标准单模光纤（直径约为20 μm，腐蚀长度约为6 mm）固定在衬底上，采用紫外臭氧清洗机（上海众濒科技有限公司，CCI UV250-MC）处理绝缘层PMMA 15 min以改善其亲水性，再通过纳米球自组装的方法[19]将PS微球（Bangs labs，PS03N）转移到光纤上，随后在PS微球上滴涂用Hummers方法[20]制备的GO溶液；3）利用高导电性银墨水沉积一层电极层，通过银丝将GPI器件的电极引出并将其与印刷电路板（PCB）相连，再利用双通道系统源表（深圳佳捷伦电子仪器有限公司，Keithley2612）对PCB加电，从而实现对该器件施加调制电压，最后根据去包层的光纤的长度和GO/PS复合材料的尺寸，可以估算出调制器的实际光电相互作用区域约为4 mm×6 mm。

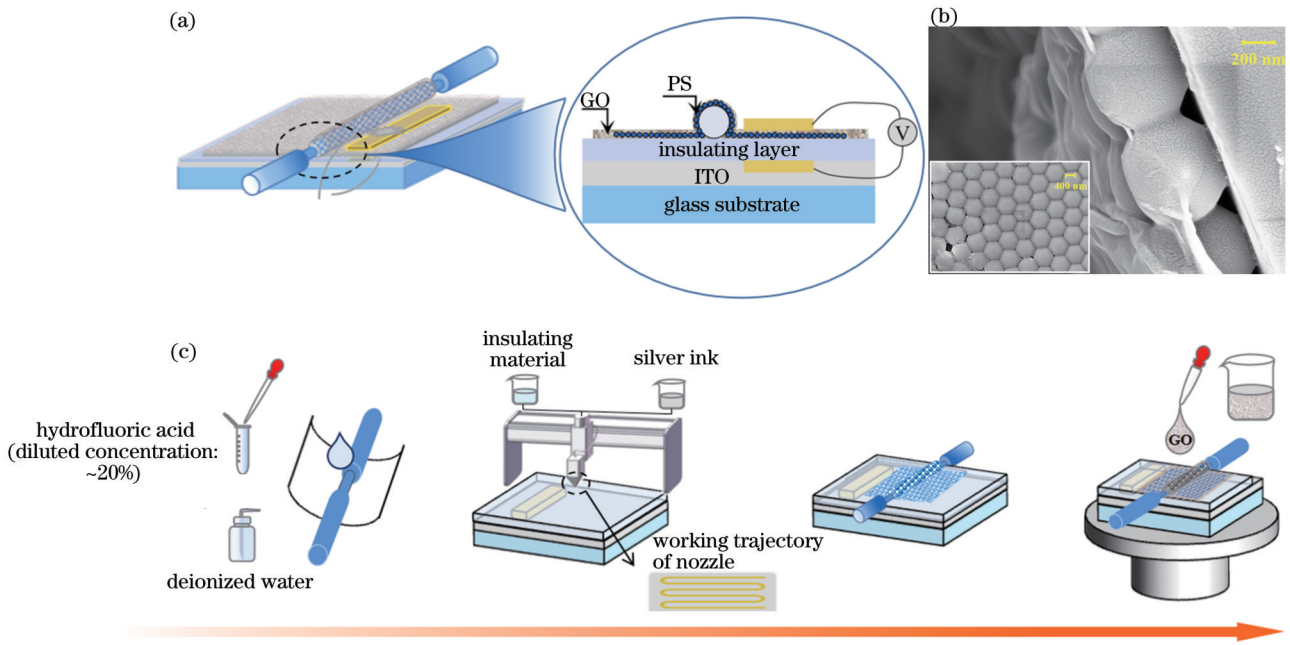

图1　GPI器件的结构和制备工艺示意图。(a) GPI器件的结构示意图；(b) GO/PS复合材料的截面SEM图像（插图为俯视面SEM图像）；(c)制备GPI器件基本的工艺流程图

Fig. 1　Schematic diagram of GPI device structure and preparation process. (a) Schematic diagram of GPI device structure; (b) SEM image of cross section of GO/PS composite material (inset is top-view SEM image); (c) basic process flow chart for preparing GPI device

图 2(a)展示了 GO C1s 区的 X 射线光电子能谱分析(XPS)图像。可以看到,C—C、C—OH、C═O 和 O═C—OH 结构的结合能依次为 285.9 eV、288.0 eV、289.8 eV 和 292.3 eV,基本符合 GO 的 XPS 结果[21]。对比石墨烯的 XPS 图像[22]可知,GO 中含氧官能团峰值的相对强度都明显增加了,这也证实了 O 原子的掺入改变了石墨烯的结构。GO 的拉曼光谱图如图 2(b)所示,包括分别在 1340.90 cm^{-1} 和 1592.70 cm^{-1} 拉曼频移处的 D 峰和 G 峰。其中,D 峰相对于石墨烯有所增强,这证实了含氧官能团的存在使 sp^2 向 sp^3 碳杂化方式转变,符合其拉曼光谱特征[23]。2D 峰的存在表明样品并未被完全氧化,它的宽度和强度都说明了利用自制的 GO 溶液滴涂制备的表征样品是由少层 GO 组成的薄膜[24]。正如图 2(b)中左上角插图所示的 GO 的 SEM 图像,石墨烯被氧化而形成了卷皱的层状结构。

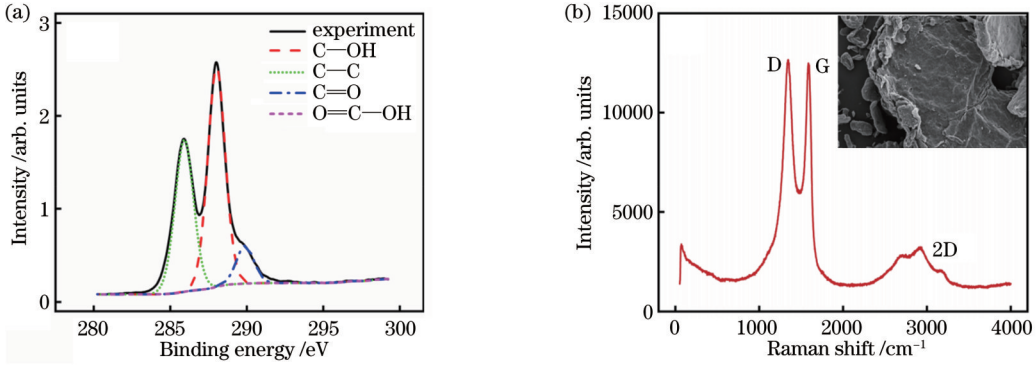

图 2　GO 的表征图。(a) GO 的 XPS 图像;(b) GO 的拉曼光谱图(插图为 GO 的 SEM 图像)

Fig. 2　Representation diagram of GO. (a) XPS image of GO; (b) Raman spectrum of GO (inset is SEM image of GO)

3　器件的调制原理分析

为了深入了解 GPI 器件光学吸收特性发生变化的原因,从微观角度分析了器件的电调制工作原理。GO 的原子结构如图 3(a)所示,其中 ρ 为电势。当施加驱动电压时,电子从石墨烯的底部转移到上方,甚至可以进一步转移到吸附的氧原子上。这种电荷转移导致 GO 两侧出现电子的积累与耗散现象,从而使其上下层表现出不同的电场强度。整个系统的总能量增加,且 GO 两侧不对称的电子浓度使其光电性能发生了变化[25]。GO 中 sp^3 碳团簇边界所引起的无序诱导结构直接影响了电子的局域态密度分布,受驱动电压影响,局域态密度因极性含氧基团的极化效应而发生变化。当 GO 作为可饱和吸收介质时,改变其电子局域态密度分布可以使其光学吸收特性发生变化[26]。

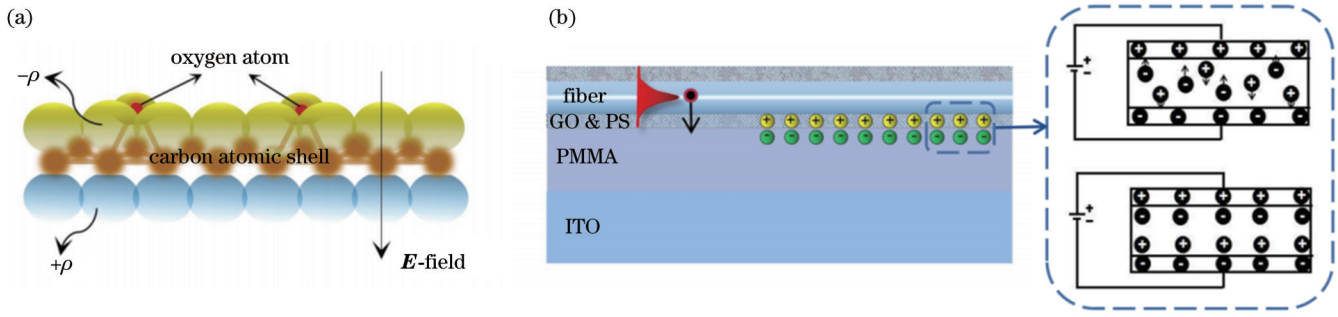

图 3　GO 的电调制原理。(a) GO 原子结构上电子的积累与耗尽;(b)外加电场影响 GPI 器件的微观示意图

Fig. 3　Electromodulation principle of GO. (a) Accumulation and depletion of electrons in GO atomic structure; (b) microscopic diagram of applied electric field affecting GPI device

从 GPI 器件的整体角度分析,外加驱动电压会使分界面上出现电荷移动,此时离子在分界面上形成双电层(EDL)结构,如图 3(b)所示。双电层的电容结构导致 GO 内部载流子浓度发生变化。从理论上讲,载流子浓度由化学势决定[27],表达式为

$$n_s=\frac{2}{\pi h^2 v_F^2}\int_0^{\infty}\varepsilon f\left[{}_d(\varepsilon)-f_d(\varepsilon+2\mu_c)\right]\mathrm{d}\varepsilon, \quad (1)$$

式中:h 是普朗克常量;v_F 是材料中狄拉克费米子的费米速度;ε 是能量;μ_c 是化学势;$f_d(\varepsilon)=\left[\exp\left(\frac{\varepsilon-\mu_c}{K_BT}\right)+1\right]^{-1}$ 是费米-狄拉克分布;K_B 是玻尔兹曼常数。材料的化学势和外加电压有直接的关系[28],定义为

$$\mu_c = h v_F \sqrt{n\pi |V - V_{Dirac}|}, \tag{2}$$

式中：η是电压作用下材料层间的平板电容常数；V_{Dirac}是材料掺杂造成的补偿电压；V为外加电压。为简化公式，将$|V - V_{Dirac}|$视为外加偏置电压。半导体材料的直接带间跃迁的光学吸收系数[29]可以写成

$$\alpha = \alpha_0 \left[f_1(1 - f_2) - f_2(1 - f_1) \right], \tag{3}$$

式中：f_1和f_2分别为载流子在初始态（价带）和最终态（导带）的占据概率；α_0为初始吸收系数。因此，通过改变外加电压的方式调节GO的化学势，进而改变GO的载流子浓度，最终可实现其光学吸收特性的改变。

然而，GO的吸收能力有限，其与倏逝光的有效作用区域受限于器件的规格。因此，为提升GPI器件的调制效率，使用了GO材料和PS纳米微球结合的方法。如图4所示，基于光波导原理，光纤中泄漏出的倏逝光会被局限在GO/PS微球内形成局域场，从而提高了倏逝光的有效利用率。在外加电场作用下，电子会聚集在GO和PS微球的分界面上，形成了界面极化现象[30]。电子的集聚会让该处的局域场在一定程度上相对增强[31]，从而提高了器件的调制效率。

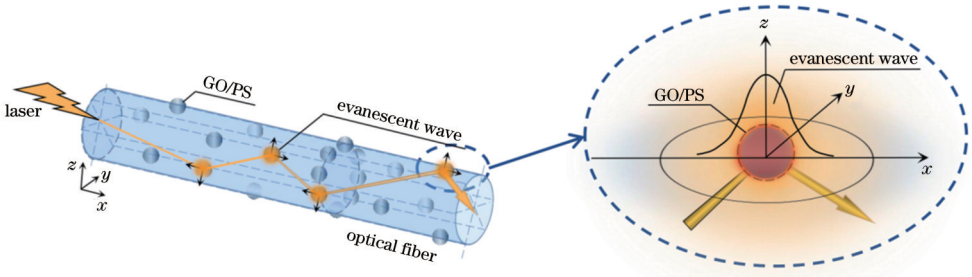

图4　光纤中光传输示意图和单个GO/PS局域场示意图

Fig. 4　Schematic diagrams of optical transmission in fiber and single GO/PS local field

为了更好地检测器件的性能，本文测量了器件的光学特性曲线。图5(a)展示了在0、20、−20 V三种电压下，GPI器件的光传输效率曲线。结果显示，在施加驱动电压时，GPI器件对1550 nm处的光吸收能力提前达到饱和，故光传输效率相对增强。同时，观察到在正负电压下，GPI器件产生了不同的光传输效率。因此，本文测试了在低泵浦功率(35 mW)下，器件的光传输能力随调制电压的变化曲线，如图5(b)所示。结果证明，在施加驱动电压后，GO内部载流子浓度增加，其介电常数的提升使得调制器的光传输能力变强。此外，由于器件中的GO在制备过程中掺杂了载流子，表现出轻微的n型半导体的性质，故该器件在正向电压下表现出更有效的调制效率，从而使器件在20 V正向驱动电压下的光传输能力就达到了−60 V电压所产生的效果。

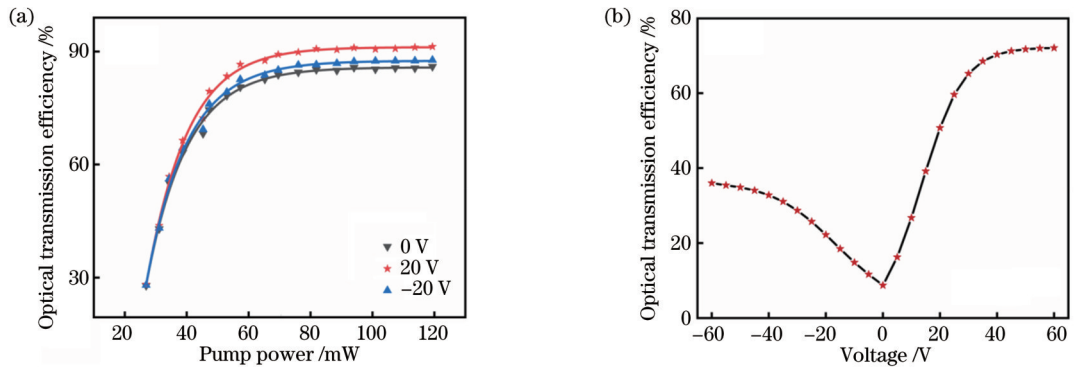

图5　GPI器件的光学特性曲线。(a)不同驱动电压下器件的光传输效率随泵浦功率的变化曲线；(b)在35 mW的低泵浦功率下不同驱动电压对器件光传输效率的影响

Fig. 5　Optical characteristic curves of GPI device. (a) Optical transmission efficiency of device varying with pump power under different driving voltages; (b) effect of different driving voltages on optical transmission efficiency of device at low pump power of 35 mW

4　器件的应用研究

为了研究GPI器件的电调制特性，实验中搭建了一个全光纤环形锁模激光器，结构示意图如图5所示。激光器由一个980 nm的半导体激光器(II-VI Incorporated，CM97-750-7*)、一段5.5 m长的掺铒光纤、一个内含980/1550 nm波分复用器兼容光隔离器的集成管、一个激光输出比例为20%的输出耦合器和一个基于GO/PS的电容式可饱和吸收器组成。其中，980 nm的半导体激光器通过波分复用器将泵浦光输入到激光腔中。利用集成管中的光隔离器控制激光腔中的光单向传输，使光纤回波反射的光能被有效隔离

而不影响其谐振。随着内腔功率的增加和驱动电压的改变，使用光谱分析仪、数字示波器、功率计、自相关仪和频谱分析仪获取锁模脉冲信号的相关信息，如光谱、重复频率、输出功率和脉冲宽度等。

实验将GPI器件应用于环形光纤激光器中，通过与热功率探头相连的触摸屏功率计（Thorlabs，PM200）测量其平均输出功率与吸收泵浦功率之间的关系。如图7（a）所示，整个环形激光腔中的平均输出功率随泵浦功率呈线性增长。随着泵功率的增加，在泵功率约为21 mW时出现1557.8 nm的CW激光信号。另外，当吸收泵浦功率为88.56 mW时，激光器运转模式为CWML，平均输出功率约为3.41 mW。

GPI调制器通过施加驱动电压来调控GO的非线性光学吸收特性，从而改变锁模激光系统的腔内损耗，实现激光器运转模式的调控。因此，首先研究了GPI器件的插入损耗随驱动电压的变化趋势。如图7（b）所示，在20 V的正偏电压下，器件的插入损耗从2.30 dB降低到了0.86 dB。外加垂直电场会使器件的分界面上出现电荷转移，离子因界面极化效应形成双电层结构。双电层的电容导致GO内部载流子浓度发生变化，GO的费米能级会根据偏压上下移动。泡利阻塞效应会使得光子的带间跃迁受到阻碍，从而导致GO的光子吸收下降，降低器件的插入损耗[32]。因此，在吸收泵浦功率恒定（34.3 mW）的情况下，激光器的输出功率随着器件插入损耗的降低而增大。

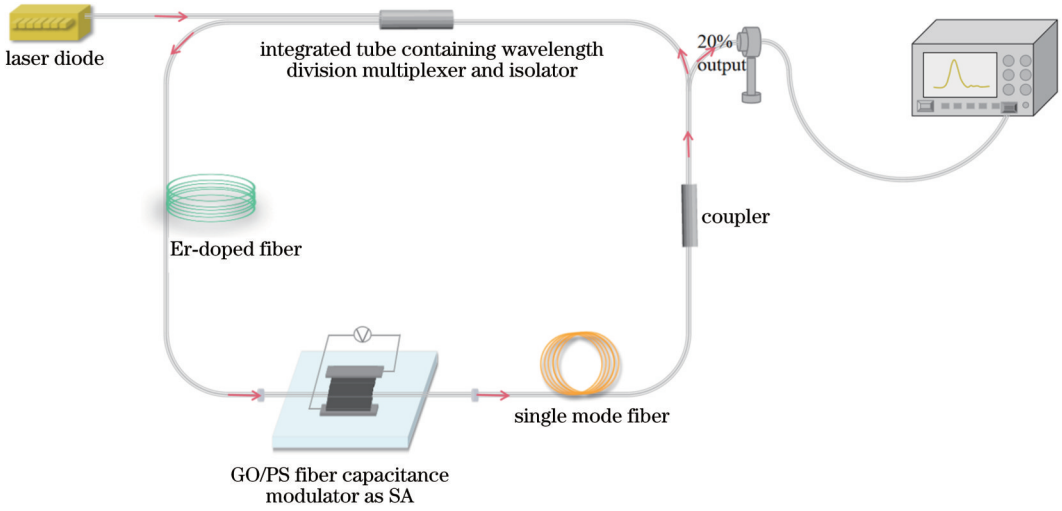

图6　基于GO/PS电光调制器的全光纤环形锁模激光器

Fig. 6　All-fiber ring mode-locked laser based on GO/PS electro-optic modulator

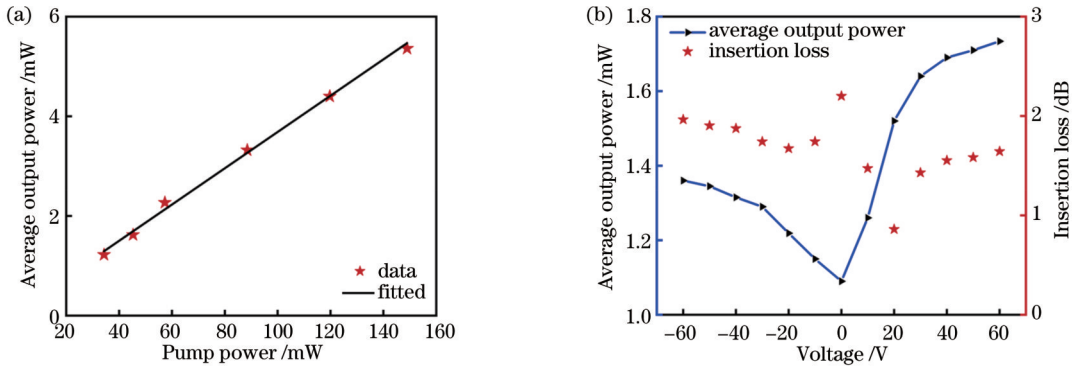

图7　全光纤激光器的输出功率。（a）平均输出功率与泵浦功率的对应关系；（b）在34.3 mW的低泵浦功率下施加电压对输出功率和器件插入损耗的影响

Fig. 7　Output power of all-fiber laser. (a) Correspondence between average output power and pump power; (b) effect of applied voltage on output power and device insertion loss at low pump power of 34.3 mW

将GPI器件集成到环形腔中，激光器产生的脉冲由快速光电二极管（Newport，818-BB-21）接收，并由带宽为500 MHz的数字示波器（Agilent，MSO7052B）记录。如图8（a）所示，当泵浦功率为34.3 mW时，数字示波器中没有显示脉冲序列，自相关仪中也未检测出脉冲信号。因此，激光器输出CW激光信号，此时并没有实现锁模脉冲输出。为了测试该可饱和器件的电调制性能，将泵浦功率稳定在34.3 mW。当给调制器施加10 V驱动电压时，谐振腔内能量提高但不足以支持激光器输出CWML信号，故激光器输出QML信

号。当继续增加调制电压到20 V时，GO内部载流子浓度的变化使GPI器件在谐振腔内产生较低的损耗和较高的能量，这进一步改善了激光器谐振腔的不稳定状态，将激光器的CW信号转换成了CWML信号[32-33]。如图8(b)所示，激光器输出稳定的CWML脉冲信号，平均输出功率为1.52 mW。采用商业自相关仪(Femtochrome Research，FR-103HP)测量激光器输出的自相关曲线，如图8(c)所示。测量结果显示，GPI器件的锁模脉冲的最窄脉冲宽度为20 ps。计算得到电调制GPI器件产生的CWML信号的时间带宽积约为1.16，该值大于高斯脉冲的转换限制值0.441，说明CWML脉冲是啁啾的。

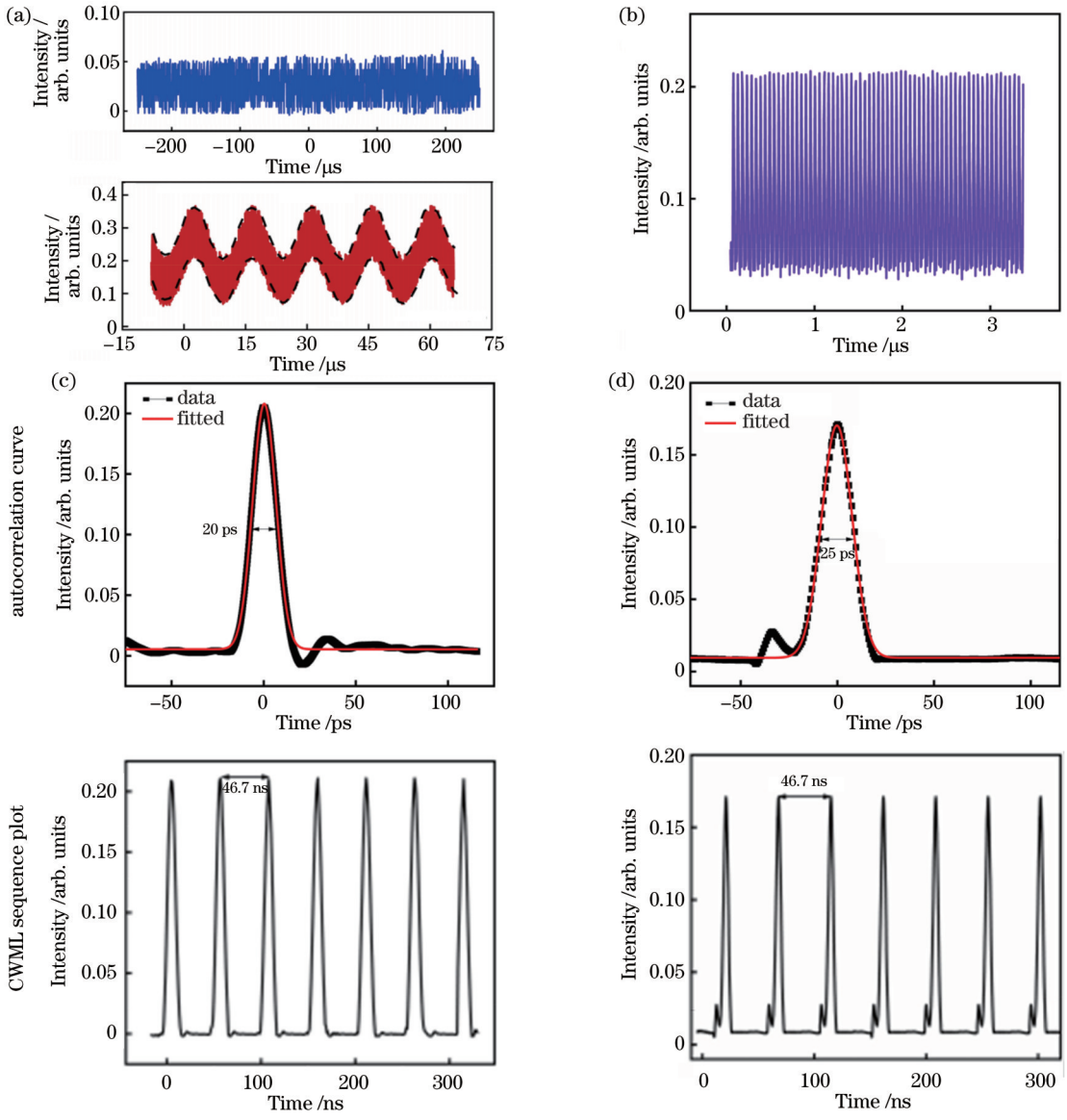

图8　不同运转条件下的脉冲序列图。(a)选用GO/PS结构后泵浦功率为34.3 mW时0 V电压下的CW信号和10 V电压下的QML信号；(b)选用GO/PS结构后泵浦功率为34.3 mW时20 V电压下的CWML信号；(c)选用GO/PS结构后泵浦功率为34.3 mW时20 V电压下的自相关曲线和CWML序列图；(d)选用GO结构后泵浦功率为44.05 mW时30 V电压下的自相关曲线和CWML序列图

Fig. 8　Pulse sequence diagrams under different working conditions. (a) CW signal at voltage of 0 V and QML signal at voltage of 10 V for pump power of 34.3 mW after using GO/PS structure; (b) CWML signal at voltage of 20 V for pump power of 34.3 mW after using GO/PS structure; (c) autocorrelation curve and CWML sequence plot at voltage of 20 V for pump power of 34.3 mW after using GO/PS structure; (d) autocorrelation curve and CWML sequence plot at voltage of 30 V for pump power of 44.05 mW after using GO structure

为了凸显GPI器件的性能，同时制备了基于GO的电容式全光纤电调制器件放入环形腔中进行对比测试。尽可能地保证了光纤纤芯、PMMA膜厚、GO膜厚和电极大小等参数的一致性。在泵浦功率为44.05 mW(此时激光器输出CW信号)时，施加30 V驱动电压后激光器输出CWML脉冲信号。此时，平均

输出功率为1.8 mW，自相关仪检测得到的锁模脉冲的最窄脉冲宽度为25 ps。通过对比发现，增加一层PS纳米微球可以实现以较小的驱动电压达到激光器运转模式可切换的要求。该现象可以解释为施加驱动电压增强了GO/PS处的局域场，使得更强的倏逝光与GO相互作用。因此，在较小的驱动电压下，调制效率的提升使激光器实现了从CW激光信号到CWML脉冲信号的转换。

图9展示了当泵浦功率稳定在34.3 mW、驱动电压为20 V时，搭建的全光纤环形锁模激光器的稳态输出特性。实验使用分辨率为0.25 nm的光纤光谱仪（Mantech，S3000-VIS）测量了激光光谱，如图9（a）所示。测量得到的激光的中心波长为1557.8 nm，半峰全宽（FWHM）为0.47 nm。射频光谱用于检测锁模激光器的稳定性，使用频谱仪（ESAd402B）测量了频率为21.4 MHz的脉冲激光的射频信号。如图9（b）所示，测量的射频信号的信噪比（R_{SN}）约为60 dB。

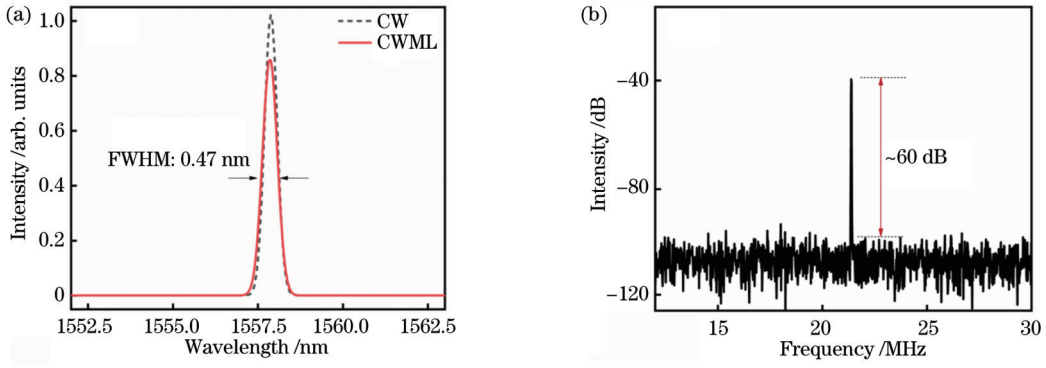

图9　全光纤锁模激光器在泵浦功率为34.3 mW、驱动电压为20 V时的输出特性。（a）光谱图；（b）频谱图

Fig. 9　Output characteristics of all fiber mode-locked laser with pump power of 34.3 mW and driving voltage of 20 V. (a) Spectrogram; (b) spectrum diagram

表1列举了所设计激光器与近年来基于各类调制器的光纤锁模激光器的性能参数。可以看出，基于GPI器件的激光器具有较低的光功率损耗，并且在较低的泵浦功率下实现了CW、QML、CWML信号的三种模式切换。然而，所设计的激光器的脉冲宽度略大于其他锁模激光器，下一步将继续优化GPI器件结构以提高调制器的调制效率，辅以适当的色散补偿技术后有望进一步压缩脉冲宽度。

表1　基于各类调制器的光纤锁模激光器的参数对比

Table 1　Parameter comparison of fiber mode-locked lasers based on various modulators

Structure	Pump power of electronically controlled ML /mW	Optical power penalty /%	Center wavelength /nm	Repetition rate /MHz	FWHM /nm	Pulse width /ps	Use of modulator	Ref.
GO/PS based capacitor	34.3	9.4	1557.8	21.40	0.47	20.00	Three operation modes switching	Our work
Graphene based field effect transistor	129.0	12.9	1559.2	4.35	1.80	1.44	Active ML	[34]
SWCNT based field effect transistor	90.0	55.5±0.6	1558.0	50.00	7.60	0.60	Two operation modes switching	[35]
Optically controlled in-line graphene SA	800.0 (1550 nm), 42.0 (980 nm)		1570.0	5.09	2.60	0.98	Three operation modes switching	[36]

为检测该器件在锁模激光器中长时间工作下的稳定性，保持泵浦功率在34.3 mW，每20 min记录一次在20 V驱动电压下激光器输出CWML脉冲时的平均输出功率。如图10所示，用功率计记录了180 min内激光器平均输出功率的变化情况，其抖动幅度为−0.5%～0.5%。

5　结　　论

介绍了一种利用微电子打印工艺制备的基于GO/PS的电容式电光调制器件，并通过XPS、SEM和拉曼光谱图分析其材料特性。在无需改变材料基本属性的情况下，通过调控驱动电压的方式就可以实现对GO吸收特性的调节，这归因于GO中载流子浓度受电场影响发生变化。由于这种电调制器件与光纤具有兼

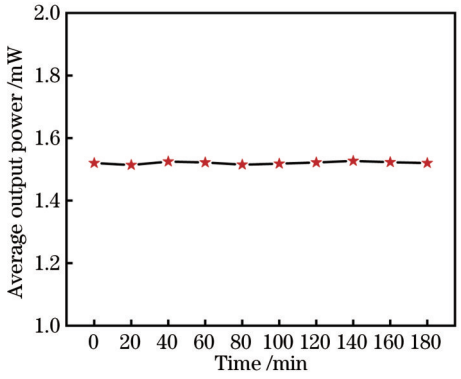

图 10 全光纤锁模激光器在泵浦功率为 34.3 mW、驱动电压为 20 V 时 180 min 内的平均输出功率曲线

Fig. 10 Average output power curve of all-fiber mode-locked laser in 180 min at pump power of 34.3 mW and driving voltage of 20 V

容性，故其可以轻松集成到所有光纤激光系统中。保持激光泵浦功率(34.3 mW)不变，通过改变驱动电压(0～20 V)的方式成功地实现了激光器运转模式(CW、QML、CWML)的切换。该器件将锁模信号的脉冲宽度压缩到了 20 ps，对应的重复频率为 21.4 MHz。根据泡利阻塞效应，GO 的光子吸收下降会使器件的插入损耗降低，此时激光器的输出功率会增大。因此，调控驱动电压可使器件的插入损耗从 2.30 dB 降低到 0.86 dB，平均输出功率从 1.09 mW 提升到 1.52 mW。鉴于所设计器件的兼容性和 GO 的宽吸收光谱范围，可进一步优化所设计器件的性能参数，为脉冲激光器的发展和应用作出贡献。

参 考 文 献

[1] 李昊, 黄威, 裴闻喜, 等. 连续波 1.7 μm 全光纤气体拉曼激光光源[J]. 光学学报, 2021, 41(3): 0314001.
Li H, Huang W, Pei W X, et al. Continuous-wave 1.7 μm all-fiber gas Raman laser source[J]. Acta Optica Sinica, 2021, 41(3): 0314001.

[2] 董文乾, 郝强, 黄坤, 等. 基于全保偏光纤激光器的单通光参量中红外超短脉冲激光系统[J]. 光学学报, 2021, 41(12): 1236001.
Dong W Q, Hao Q, Huang K, et al. Single-pass optical parameter mid-infrared ultra-short pulse laser system based on all polarization-maintaining fiber laser[J]. Acta Optica Sinica, 2021, 41(12): 1236001.

[3] 韩冬冬, 张佳月, 高琼, 等. 可切换多波长全光纤被动锁模光纤激光器[J]. 光学学报, 2021, 41(5): 0506002.
Han D D, Zhang J Y, Gao Q, et al. Switchable multi-wavelength passively mode-locked all-fiber lasers[J]. Acta Optica Sinica, 2021, 41(5): 0506002.

[4] 董自凯, 宋晏蓉. 光纤激光器被动锁模技术研究进展[J]. 中国激光, 2021, 48(5): 0501006.
Dong Z K, Song Y R. Research progress of mode-locked fiber lasers based on saturable absorbers[J]. Chinese Journal of Lasers, 2021, 48(5): 0501006.

[5] Lu B L, Fang Y, Lü C Y, et al. Single- and bound-state soliton mode-locked Er-doped fiber laser based on graphene/WS_2 nanocomposites saturable absorber[J]. Infrared Physics & Technology, 2022, 121: 104024.

[6] Wang S K, Tu C R, Mahabadi S E J, et al. Obtaining more energetic modelocked pulses from a SESAM-based fiber laser [J]. Optics Express, 2020, 28(14): 20345-20361.

[7] Zhang C X, Chen Y, Fan T J, et al. Sub-hundred nanosecond pulse generation from a black phosphorus *Q*-switched Er-doped fiber laser[J]. Optics Express, 2020, 28(4): 4708-4716.

[8] Zhao F Y, Wang Y S, Wang Y G, et al. Graphene oxide-COOH as a new saturable absorber for both *Q*-switching and mode-locking fiber lasers[J]. Chinese Optics Letters, 2017, 15(10): 101402.

[9] Baylam I, Cizmeciyan M N, Ozharar S, et al. Femtosecond pulse generation with voltage-controlled graphene saturable absorber[J]. Optics Letters, 2014, 39(17): 5180-5183.

[10] Jin Y, Zhou L, Liang J, et al. Electrochemically driven dynamic plasmonics[J]. Advanced Photonics, 2021, 3(4): 044002.

[11] Gao Y, Qin C B, Qiao Z X, et al. Imaging and spectrum of monolayer graphene oxide in external electric field[J]. Carbon, 2015, 93: 843-850.

[12] Nair V, Kumar A, Subramaniam C. Exceptional photoconductivity of poly(3-hexylthiophene) fibers through *in situ* encapsulation of molybdenum disulfide quantum dots[J]. Nanoscale, 2018, 10(22): 10395-10402.

[13] Kovalchuk O, Uddin S, Lee S, et al. Graphene capacitor-based electrical switching of mode-locking in all-fiberized femtosecond lasers[J]. ACS Applied Materials & Interfaces, 2020, 12(48): 54005-54011.

[14] Lee E J, Choi S Y, Jeong H, et al. Active control of all-fibre graphene devices with electrical gating[J]. Nature Communications, 2015, 6: 6851.

[15] Baylam I, Özharar S, Kakenov N, et al. Femtosecond pulse generation with voltage-controlled graphene saturable absorbers [M]//Binder R. Optical properties of graphene. Singapore: World Scientific, 2016: 389-433.

[16] 丁烨, 李强, 李靖怡, 等. 超快激光在无源光波导器件制造中的应用综述[J]. 中国激光, 2021, 48(8): 0802020.
Ding Y, Li Q, Li J Y, et al. Application of ultrafast lasers in the manufacture of passive optical waveguide devices: a review[J]. Chinese Journal of Lasers, 2021, 48(8): 0802020.

[17] Lian T H, Yang K D, Wang X B, et al. Electro-absorption optical modulator based on graphene-buried polymer waveguides [J]. IEEE Photonics Journal, 2020, 12(4):6601610.

[18] Osicka J, Mrlik M, Ilcikova M, et al. Controllably coated graphene oxide particles with enhanced compatibility with poly(ethylene-co-propylene) thermoplastic elastomer for excellent photo-mechanical actuation capability[J]. Reactive and Functional Polymers, 2020, 148: 104487.

[19] Zhang K, Zhang W L, Choi H J. Facile fabrication of self-assembled PMMA/graphene oxide composite particles and their electroresponsive properties[J]. Colloid and Polymer Science, 2013, 291(4): 955-962.

[20] Hou Y G, Lü S H, Liu L P, et al. High-quality preparation of graphene oxide via the Hummers′ method: understanding the roles of the intercalator, oxidant, and graphite particle size[J]. Ceramics International, 2020, 46(2): 2392-2402.

[21] Chien C T, Li S S, Lai W J, et al. Tunable photoluminescence from graphene oxide[J]. Angewandte Chemie, 2012, 51(27): 6662-6666. [PubMed]

[22] Al-Gaashani R, Najjar A, Zakaria Y, et al. XPS and structural studies of high quality graphene oxide and reduced graphene oxide prepared by different chemical oxidation methods[J]. Ceramics International, 2019, 45(11): 14439-14448.

[23] Qiao Z X, Qin C B, Gao Y, et al. Modulation of the optical transmittance in monolayer graphene oxide by using external electric field[J]. Scientific Reports, 2015, 5: 14441.

[24] Kostiuk D, Bodik M, Siffalovic P, et al. Reliable determination of the few-layer graphene oxide thickness using Raman spectroscopy[J]. Journal of Raman Spectroscopy, 2016, 47(4):

391-394.
[25] Topsakal M, Gürel H H, Ciraci S. Effects of charging and electric field on graphene oxide[J]. The Journal of Physical Chemistry C, 2013, 117(11): 5943-5952.
[26] Gao Y, Qin C B, Qiao Z X, et al. Observing and tuning the density distribution of localized states of monolayer graphene oxide by using external electric field[J]. Applied Physics Letters, 2015, 106(13): 131103.
[27] Xu C, Jin Y C, Yang L Z, et al. Characteristics of electro-refractive modulating based on graphene-oxide-silicon waveguide [J]. Optics Express, 2012, 20(20): 22398-22405.
[28] Hanson G W. Dyadic Green's functions for an anisotropic, non-local model of biased graphene[J]. IEEE Transactions on Antennas and Propagation, 2008, 56(3): 747-757.
[29] Zitter R N. Saturated optical absorption through band filling in semiconductors[J]. Applied Physics Letters, 1969, 14(2): 73-74.
[30] Islam R, Papathanassiou A N, Chan-Yu-King R, et al. On the sign of the relaxation activation energy for interfacial polarization in reduced graphene oxide-based nano-composites[J]. Applied Physics Letters, 2016, 109(18): 182901.
[31] Fernandes D E, Pereira R A M, Lannebère S, et al. Experimental verification of ill-defined topologies and energy sinks in electromagnetic continua[J]. Advanced Photonics, 2022, 4(3): 035003.
[32] Baylam I, Balci O, Kakenov N, et al. Graphene-gold supercapacitor as a voltage controlled saturable absorber for femtosecond pulse generation[J]. Optics Letters, 2016, 41(5): 910-913.
[33] Baylam I, Ozharar S, Kakenov N, et al. Femtosecond pulse generation from a Ti^{3+}: sapphire laser near 800 nm with voltage reconfigurable graphene saturable absorbers[J]. Optics Letters, 2017, 42(7): 1404-1407.
[34] Bogusławski J, Wang Y D, Xue H, et al. Graphene actively mode-locked lasers[J]. Advanced Functional Materials, 2018, 28 (28): 1801539.
[35] Gladush Y, Mkrtchyan A A, Kopylova D S, et al. Ionic liquid gated carbon nanotube saturable absorber for switchable pulse generation[J]. Nano Letters, 2019, 19(9): 5836-5843.
[36] Gene J, Park N H, Jeong H, et al. Optically controlled in-line graphene saturable absorber for the manipulation of pulsed fiber laser operation[J]. Optics Express, 2016, 24(19): 21301-21307.

Fiber Laser with Switchable Operating Modes Based on Graphene Oxide/Polystyrene Electro-Optic Modulator

Zhang Xiaoying[1], Chang Jianhua[1,2*], Dai Tengfei[1,2], Su Youpeng[1], Liu Xiang[1], Ni Haibin[1]

[1]*School of Electronics & Information Engineering, Nanjing University of Information Science & Technology, Nanjing* 210044, *Jiangsu, China*;

[2]*Collaborative Innovation Center of Atmospheric Environment and Equipment Technology, Nanjing University of Information Science & Technology, Nanjing* 210044, *Jiangsu, China*

Abstract

Objective Short-pulse fiber lasers have attracted great interest in numerous fields, including fiber communication, laser medical treatment, bioengineering, and material processing, owing to their compact structure, high efficiency, and robust stability. Physically, mode locking is an effective method to obtain ultrashort pulses, and it can be divided into active mode locking and passive mode locking. Passive mode locking based on saturable absorbers (SAs) has been widely studied. Among the SA materials, two-dimensional (2D) materials, such as graphene, black phosphorus, and molybdenum disulfide (MoS_2), are promising candidates due to their distinctive nonlinear saturable absorption ability, ultrafast recovery rate, and low cost. Plenty of passively mode-locked fiber lasers based on 2D materials have been developed to achieve different operating modes, such as continuous wave, *Q*-switched mode locking, and continuous wave mode locking by changing the pump power. However, due to the relatively fixed optical absorption characteristics of 2D materials, switchable operating modes of a mode-locked laser system are difficult to achieve without external modulation. The present study reports a novel kind of electro-optic modulator that is composed of graphene oxide (GO) and polystyrene (PS) microspheres and exhibits adjustable absorption characteristics under the action of an external electric field. The designed modulator, with a high optical transmission capability, enables electrically modulated fiber lasers to be switched among various operating modes, including continuous wave, *Q*-switched mode locking, and continuous wave mode locking. The proposed basic strategy and findings are expected to facilitate the design of new switchable ultrashort-pulse lasers based on electro-optic modulators.

Methods The GO/PS all-fiber capacitive device is mainly prepared on a quartz substrate by the microelectronic printing process, and the main preparation process is presented in Fig. 1. Improving the modulation efficiency of the device requires a straightforward, low-cost, and effective approach in which PS microspheres can enhance the interaction area between the laser and the material by creating a local field to restrict the divergence of the evanescent light. The modulation characteristics of the modulator can be studied by measuring the optical characteristic curve of the device. The

results show that the saturated absorption by the GO in the modulator can easily be achieved at 1550 nm when the driving voltage is applied, indicating enhanced optical transmission efficiency. Finally, an all-fiber mode-locked ring laser system is studied and constructed. The operating mode of the laser can be actively switched by integrating the device with the laser system and applying different electrical fields.

Results and Discussions The light absorption intensity of the all-fiber capacitive device based on the GO/PS composite increases with the driving voltage [Fig. 5 (a)], which indicates that the absorption characteristics of the device can be effectively adjusted by the electrical field. The feasibility of the experiment is also verified. To further observe the difference in the optical transmission efficiency of the device under positive and negative voltages, the variation in the optical transmission capability of the device with the driving voltage under a low pump power (35 mW) is tested [Fig. 5 (b)]. The results show that the device achieves higher modulation efficiency under the positive voltage due to the properties of n-type semiconductors caused by slight doping. The nonlinear optical absorption characteristics of the GO in the modulator can be adjusted by the driving voltage, and the intracavity loss can thereby be modified. On this basis, the variation of the insertion loss of the GO/PS modulator is studied when the driving voltage increases from −60 V to 60 V. As the positive bias voltage reaches up to 20 V, the insertion loss of the device is reduced from 2.30 dB to 0.86 dB [Fig. 7 (b)]. Then, the device is applied to the all-fiber mode-locked ring laser system (Fig. 6). The results show that the laser achieves the switching among three operating modes: continuous wave, *Q*-switched mode locking and continuous wave mode locking under a certain range of the modulation voltage (a range from 0 V to 20 V). This all-fiber electro-optic modulator also reduces the pulse width of the mode-locked signal to 20 ps. Radio-frequency (RF) spectral measurements are conducted to characterize the stability of the fiber laser. The RF spectra of the mode-locked laser are measured [Fig. 9 (d)]. The signal-to-noise ratio (SNR) of the RF signal can reach up to around 60 dB at 21.40 MHz. To further verify the stability of the laser, the average output power of the laser in 180 minutes is measured (Fig. 10). According to the results, the all-fiber mode-locked ring laser based on the GO/PS electro-optic modulator can work steadily for a long time.

Conclusions This study presents the preparation, characterization, and analysis of a novel all-fiber capacitive device based on the GO/PS composite, which can serve as a saturable absorber in all-fiber mode-locked ring laser systems. Due to the variation of chemical potential and internal carrier concentration of the GO, the optical absorption characteristics of the GO can be adjusted by an external electrical field. The effective interaction area between the GO and the evanescent light is strictly limited by the device specification. For this reason, an effective method of combining the GO with PS microspheres is adopted. According to the principle of optical waveguides, the evanescent light leaked from the fiber is confined to the GO/PS microspheres. A local field is thereby created, ultimately enhancing the effective utilization of the evanescent light. The mode switching of the laser is successfully implemented by changing the driving voltage, and the pulse width of the mode-locked pulse signal is reduced to 20 ps. In addition, the insertion loss of the device is lowered from 2.30 dB to 0.86 dB and the average output power of the laser is increased from 1.09 mW to 1.52 mW by adjusting the amplitude of the applied voltage. The proposed all-fiber capacitive device is expected to further promote the development of switchable pulsed fiber lasers due to its compatibility and high modulation efficiency.

Key words lasers; mode-locked fiber lasers; electro-optic modulators; mode switching; graphene oxide; polystyrene